**Title page**

**Manuscript Title**

Shaping information processing: the role of oscillatory dynamics in a working-memory task

**Abbreviated Title**

The role of oscillatory dynamics in a working-memory task

**Author names & Affiliations**

Hesham A. ElShafei[1], Ying Joey Zhou[1], Saskia Haegens[1,2,3]

[1] Donders Institute for Brain, Cognition & Behavior, Radboud University, Nijmegen, The Netherlands, 6525 EN

[2] Dept. of Psychiatry, Columbia University, New York, NY, USA, NY 10032

[3] Div. of Systems Neuroscience, New York State Psychiatric Institute, New York, NY, USA, NY 10032

**Author Contributions**

HE, YZ and SH Designed Research; HE and YZ Performed Research; HE and YZ Analyzed data; HE, YZ and SH Wrote the paper

**Corresponding author**

Hesham A. ElShafei, elshafeh@gmail.com

**Acknowledgements**

We would like to thank Kristina Baumgart for her assistance with data acquisition, and Luca Iemi for thoughtful comments on an earlier version of the manuscript.

**Conflict of Interest**

Authors report no conflict of interest

**Funding sources**

This work was supported by the Netherlands Organization for Scientific Research Vidi grant 016.Vidi.185.137.

**Abstract**

Neural oscillations are thought to reflect low-level operations that can be employed for higher-level cognitive functions. Here, we investigated the role of brain rhythms in the 1–30 Hz range by recording MEG in human participants performing a visual delayed match-to-sample paradigm in which orientation or spatial frequency of sample and probe gratings had to be matched. A cue occurring before or after sample presentation indicated the to-be-matched feature. We demonstrate that alpha/beta power decrease tracks the presentation of the informative cue and indexes faster responses. Moreover, these faster responses coincided with an augmented phase alignment of slow oscillations, as well as phase-amplitude coupling between slow and fast oscillations. Importantly, stimulus decodability was boosted by both low alpha power and high beta power. In summary, we provide support for a comprehensive framework in which different rhythms play specific roles: slow rhythms control input sampling, while alpha (and beta) gates the information flow, beta recruits task-relevant circuits, and the timing of faster oscillations is controlled by slower ones.

**Significance statement**

Brain oscillations reflect low-level operations, building blocks, that control the flow of information through the brain. We propose and test a novel comprehensive framework in which slow oscillations control input sampling, alpha gates information flow, beta recruits task-relevant circuits, and the timing of faster oscillations is controlled by slower ones. We collected MEG data while participants performed a visual delayed match-to-sample task with pre- & retro-cues. Phase alignment of slow oscillations, governing input sampling, indexed faster responses. Alpha/beta power, gating information flow, boosted behavior & tracked informative cues. Low alpha (gating) & high beta (circuit-setup) power boosted signal information content. This is an essential step towards a more unified framework regarding the role of oscillatory dynamics in shaping information processing.

## 1 Introduction

Brain oscillations reflect rhythmic fluctuations of neuronal ensembles between states of low and high excitability (Bishop, 1932). Earlier research focused on investigating oscillations independently and linking them to high-level cognitive processes (e.g., theta to memory). However, this approach has been critiqued, as the exact role of each rhythm likely depends on an interplay between brain region, underlying neuronal substrate, and task context (Buzsaki, 2006; Wang, 2010). Our work is based on the hypothesis that oscillations reflect low-level mechanisms that can be flexibly employed to change the dynamics of neuronal populations, thereby providing the scaffolding for information processing. Thus, oscillations set the state of the system, either enhancing or attenuating activity (Klimesch et al., 2007), and inhibiting or facilitating network formation (Singer, 1999; Varela et al., 2001). Here, we focus on oscillations in the delta-to-theta, alpha, and beta bands in the context of working-memory.

Slow rhythms in the delta-to-theta bands have been proposed to govern the sampling of our surroundings by providing alternating phases of high and low neural excitability and thereby phases of high and low perceptual sensitivity (Fiebelkorn & Kastner, 2019; Helfrich et al., 2019; Herbst & Landau, 2016; VanRullen, 2016). Accordingly, sensory processing (and subsequent behavior) depends on the temporal coincidence of task-relevant targets with the oscillatory phase; i.e., when the phase with high excitability coincides with target occurrence, neural and behavioral responses are enhanced (Busch et al., 2009; Dugué et al., 2015; Fiebelkorn et al., 2013; Henry et al., 2016; Landau & Fries, 2012; VanRullen et al., 2011; Zion Golumbic et al., 2013). It has been shown that slow oscillations also control the timing of faster oscillations through phase-amplitude coupling (Canolty et al., 2010; Meij et al., 2012; Sauseng et al., 2019). However, it

remains unclear how these cross-frequency interactions shape sensory processing and subsequent behavior. Here, we will investigate how the phase of slow rhythms, as well as coupling between slow and faster rhythms, correlates with behavior.

The alpha rhythm is thought to reflect functional inhibition (Klimesch et al., 2007), such that increased alpha power suppresses processing in task-irrelevant regions and networks (i.e., increased alpha reflects reduced neural excitability), while decreased alpha facilitates processing in task-relevant ones, effectively gating the information flow (Jensen & Mazaheri, 2010). Accordingly, it has been demonstrated that working-memory performance correlates positively with alpha activity in task-irrelevant (Haegens et al., 2010; Yu et al., 2017) and negatively in task-relevant regions (Jiang et al., 2015; van Ede et al., 2017), respectively. However, it remains unclear how alpha gating modulates internal sensory representations (as indexed by decoding performance), with studies reporting positive (i.e., decoding performance increases as alpha power increases; Kayser et al., 2016), negative (Barne et al., 2020), and null relationships (Griffiths et al., 2019). Here we will examine how alpha power correlates with working-memory performance as well as the decodability of task features.

While the beta rhythm was traditionally regarded as a somatomotor rhythm (Pfurtscheller & Lopes da Silva, 1999), recent evidence suggests that beta is involved in top-down processing (Buschman & Miller, 2007) and long-range communication (Engel & Fries, 2010). However, it is unclear onto which low-level mechanisms beta oscillations map. One proposal is that beta, like alpha, gates information processing through inhibition (Lundqvist et al., 2016; Miller et al., 2018). A more recent proposal is that beta facilitates the endogenous (re)activation of cortical content representations, e.g., during working memory (Spitzer & Haegens, 2017). In this framework, beta-

band synchronization supports the endogenous transition from latent to active cortical representations during working memory, thereby providing a readout of the information held in memory. This proposal builds primarily upon evidence from non-human primate research (Bahmani et al., 2018; Haegens et al., 2017; Salazar et al., 2012) and is yet to be explicitly tested in the human brain (Herding et al., 2016). Here we will test the involvement of beta oscillations in circuit (re)activation, the possibility of the existence of multiple beta(s), and how these tentative different betas correlate with behavior.

Combined, we propose a framework of oscillations as building blocks, in which delta-to-theta rhythms sample task-relevant input, while the alpha rhythm suppresses irrelevant input. Crucially, the beta rhythm recruits task-relevant circuits that maintain information in working memory. Finally, the timing of faster oscillations is controlled by slower rhythms via phase-amplitude coupling. Critically, we propose that oscillations (separately and combined) orchestrate the functional architecture of information processing and thereby shape behavior. In order to elucidate unsettled oscillatory characteristics (including the relationship of alpha to sensory representations and phase-amplitude coupling to behavior), we recorded MEG in healthy participants preforming a visual delayed match-to-sample working-memory paradigm with pre- and retro-cueing.

## 2 Materials & Methods

### 2.1 Participants

Participants were 33 healthy right-handed adults (21 female, 12 male; mean age 24.6 years; range 20–33) without neurological or psychiatric disorders, who reported normal hearing and normal or corrected-to-normal vision. The study was approved by the local ethics committee (CMO 2014/288 “Imaging Human Cognition”) and in accordance with the Declaration of Helsinki. Participants gave written informed consent and were remunerated for their participation.

### 2.2 Visual working-memory task

We used a single-item delayed match-to-sample working-memory task where participants were instructed to compare sample and probe stimuli and indicate whether the cued feature was the same or different between them (Figure 1). Each trial contained four main events: a visual cue followed by a visual sample, a second visual cue, and a probe. All events were presented at a fixed stimulus onset asynchrony (SOA) of 1.5 s. The inter-trial interval (ITI) duration was jittered between 2 and 2.4 s.

We used a two (relevant feature: orientation vs. frequency) by two (informative cue: pre- vs. retro-cue) factorial design. Participants were cued to compare sample and probe orientation in half of the trials, and spatial frequency in the other half. They were informed about the relevant feature by an informative cue, which occurred either before (pre; 50%) or after (retro; 50%) the sample presentation. These four trial types were randomly interleaved such that within each block participants performed all task conditions. Participants gave their response (“same” or “different”) by pressing a button with their right index or middle finger. The response-button

137 mapping changed on a block-by-block basis in order to avoid motor preparation confounds in our
138 decision-related analyses.
139 Participants first performed a few short practice sequences of the task (20 trials each) in which
140 feedback was provided on a trial-by-trial basis, with green and red fixation dots for correct and
141 incorrect responses, respectively. During the main experiment, we recorded MEG while
142 participants performed 8 blocks of 64 trials each, in which feedback was provided on a block-by-
143 block basis. The full recording session lasted around 90 minutes.

144 **2.3 Stimuli**

145 A bull's eye (outer black ring = 0.5° × 0.5° degree of visual angle (dva), innermost black dot = 0.25°
146 × 0.25° dva) was presented at the center of the screen as the fixation point. Participants were
147 instructed to always maintain fixation, and not to blink during the presentation of the stimuli.
148 Each trial started with a cue presented for 300 ms. Next, a sample consisting of an oriented
149 grating (Michelson contrast: 40%, spatial frequency: 1 cycle per °, orientation: 45° clockwise or
150 counterclockwise relative to vertical, randomized spatial phase) and a backward mask (a
151 bandpass-filtered noise patch with matched contrast and spatial frequency as the grating) were
152 presented sequentially for 230 ms. Both the grating and the mask were shown in an annulus
153 (inner radius = 1.5°, outer radius = 7.5°, contrast of the stimuli decreased linearly to 0 over the
154 outer and inner 0.5° radius of the annulus) around the central fixation (Figure 1A). After an SOA
155 of 1.5 s, a second cue was presented for 300 ms. The trial presentation finished with the probe
156 presentation, which, similar to the sample, consisted of an oriented grating and a backward mask.
157 The probe's cued feature matched with that of the sample grating in 50% of the trials. The
158 experiment was programmed with PsychtoolBox (Brainard, 1997) in Matlab (Mathworks, Inc.).

159 **2.4 Data acquisition**

160 Stimuli were displayed on a semitranslucent screen (1920 × 1080-pixel resolution, 120-Hz refresh
161 rate) back-projected by a PROpixx projector (VPixx Technologies) during MEG recordings. Whole-
162 head MEG data were acquired at a sampling frequency of 1200 Hz with a 275-channel MEG
163 system with axial gradiometers (CTF MEG Systems, VSM MedTech Ltd.) in a magnetically shielded
164 room. Six permanently faulty channels were disabled during the recordings, leaving 269 recorded
165 MEG channels. Three fiducial coils were placed at the participant's nasion and both ear canals,
166 to provide online monitoring of participant's head position (Stolk et al., 2013) and offline
167 anatomical landmarks for co-registration. Eye position was recorded using an eye tracker
168 (EyeLink, SR Research Ltd.). Upon completion of the MEG session, participant's head shape and
169 the location of the three fiducial coils were digitized using a Polhemus 3D tracking device
170 (Polhemus, Colchester, Vermont, United States). Anatomical T1-weighted MRIs were obtained
171 during a separate session. To improve co-registration of the MRIs and MEG data, earplugs with a
172 drop of Vitamin E were placed at participant's ear canals during MRI acquisition. These
173 anatomical scans were used for source reconstruction of the MEG signals.

174 **2.5 Behavioral analysis**

175 The influence of cue condition (two levels: pre- and retro-cue) and feature (two levels:
176 orientation and spatial frequency) on median reaction time (RT; including correct responses only)
177 and accuracy (percentage of correct responses) was tested using a linear mixed-effects model
178 using the lme4 package (Bates et al., 2015) for R (Team, 2014). For post-hoc analysis we used the
179 Lsmean package (Searle et al., 1980) where p-values were considered as significant at $p<0.05$ and
180 adjusted for the number of comparisons performed (Tukey method).

181 **2.6 MEG pre-processing**

182 MEG data were preprocessed offline and analyzed using the FieldTrip toolbox (Oostenveld et al.,
183 2011) and custom-built MATLAB scripts. The MEG signal was epoched based on the onset of the
184 first cue (t= -1 to 7s). The data were downsampled to a sampling frequency of 300 Hz, after
185 applying a notch filter to remove line noise and harmonics (50, 100, and 150 Hz). Bad channels
186 and trials were rejected via visual inspection before independent component analysis (Jung et
187 al., 2001) was applied. Subsequently, components representing eye-related and heart-related
188 artefacts were projected out of the data (on average, four components were removed per
189 participant). Finally, outlier trials of extreme variance were removed. This resulted in an average
190 of 393 (± 9 SEM) trials and 268 channels per participant for the reported analyses.

191 **2.7 Event-related fields**

192 Single-trial data were baseline corrected (t = −0.1 to 0 s) before calculation of first-cue and grating
193 locked event-related fields (ERFs). In addition, a planar representation of the MEG field
194 distribution was calculated from the averaged data (ERFs) using the nearest-neighbor method.
195 This transformation makes interpretation of the sensor level data easier as the signal amplitude
196 is typically maximal above a source.

197 **2.8 Spectral analysis**

198 Our analysis aimed to highlight the (1) differential impacts of pre- and retro-cueing on the
199 oscillatory dynamics of interest, and (2) the behavioral relevance of these dynamics. For both
200 these contrasts, our spectral measures included delta-to-theta inter-trial phase coherence, alpha
201 power, and beta power. For the cueing contrast, spectral measures were compared between pre-
202 and retro-cue trials (including correct response trials only). For the behavioral contrast, trials

203 from all conditions (including both correct and incorrect response trials) were pooled together
204 and divided into five quantile bins (approx. 80 trials per bin) according to RT. Spectral measures
205 were contrasted between the slowest and fastest RT bins, to maximize statistical power.
206 For the 20 MEG channels displaying the maximal post-grating ERFs (channels selected individually
207 per participant), we extracted 1-s pre-stimulus windows (t = −1 to 0 s), multiplied these with a
208 Hanning taper, and computed power spectra (1–30 Hz; 1-Hz resolution) using a fast Fourier
209 transform (FFT) approach. In order to determine the individual alpha peak frequency, we
210 detected the highest local maximum within the 7–14 Hz band. In order to detect the beta peak
211 frequency, linear regression (least-squares fit) was used to fit a linear model to the log-
212 transformed spectrum in the beta range in order to compensate for the 1/f effect. The fitted
213 linear trend was then subtracted from the spectrum, allowing for a more reliable beta peak
214 frequency estimate within the 15–30 Hz band (Haegens et al., 2014).
215 We identified distinct alpha peak frequencies for all participants (mean = 9.9 Hz ± 0.21 SEM;
216 Figure 2), while for beta we identified peaks for 18 participants (mean = 20.8 Hz ± 0.37 SEM) and
217 assigned the mean beta peak for the remainder of the participants (N=15). It is important to note
218 that our peak estimations did not significantly vary when removing the 1/f background noise (p
219 = 0.1 for alpha, p = 0.3 for beta). In order to create peak-centered signals, we computed TFRs of
220 the power spectra for the full trials per experimental condition. To this end, we used an adaptive
221 sliding time window of five cycles length per frequency (Δt = 5/f; 20-ms step size), and estimated
222 power after applying a Hanning taper. We created alpha-peak (individualized) and beta-peak
223 (individualized) centered time-resolved signals with spectral bandwidths of 2 Hz and 4 Hz,

respectively. Power normalization was performed relative to a baseline (t = -0.4 to -0.2 s) for the cueing contrast and relative to the average of all RT bins for the RT contrast.

We estimated inter-trial phase coherence (Tallon-Baudry et al., 1996) across trials, for each time point, frequency and sensor, for each RT bin separately. This measure reflects the degree to which the phase of each frequency is aligned across trials. We averaged this measure between 1 and 6 Hz in order to reduce data dimensionality. In addition, we used the Tensorpac toolbox (Combrisson et al., 2020) to compute a time-resolved measure of phase-amplitude coupling (PAC) on source level. This algorithm measures PAC across trials (rather than across time).

### 2.9 Statistical analysis

In order to investigate whether differences between conditions of interest (cueing contrast: pre- vs. retro-cue; RT contrast: slowest vs. fastest RT bin) were statistically significant, we used nonparametric cluster-based permutation analysis (Maris & Oostenveld, 2007). In brief, this test first calculates paired t-tests for each sensor at each time and/or frequency point, which are then thresholded at $p < 0.05$ and clustered on the basis of temporal, spatial and/or spectral adjacency. The sum of t-values within each cluster is retained, and the procedure is repeated 1000 times on permuted data in which the condition assignment within each individual is randomized. On each permutation, the maximum sum is retained. Across all permutations, this yields a distribution of 1000 maximum cluster values. From this distribution, the probability of each empirically observed cluster statistic can be derived (evaluated at alpha = 0.05).

### 2.10 Source reconstruction

For each participant, an anatomically realistic single-shell headmodel based on individual T1-weighted anatomical images was generated (Nolte, 2003). A grid with 0.5-cm resolution was

created using an MNI template onto which the brain volume of each participant was morphed using non-linear transformation. For each grid point, leadfields were computed with a reduced rank, which removes the sensitivity to the direction perpendicular to the surface of the volume conduction model. This procedure ensures that each grid point represents the same anatomical location across all participants.

In order to visualize the sources of our sensor-level spectrotemporal (power and ITC) and temporal effects (ERFs), we utilized the frequency-domain adaptive spatial technique of dynamical imaging of coherent sources (DICS; Gross et al., 2001) and the linearly constrained minimum variance beamformer (LCMV; Van Veen et al., 1997), respectively. Data from all conditions of interest were concatenated in order to compute the cross-spectral density (CSD) matrices (t= -1 to 2 s; multitaper method (Mitra & Pesaran, 1999)) and the covariance matrices of the averaged single trials (t= -0.6 to 5.5 s; lambda 5%) for the DICS and LCMV beamformer, respectively. Leadfields for all grid points along with the CSD/covariance matrices were used to compute a common spatial filter (i.e., common for all trials and conditions) that was used to estimate the spatial distribution of power/amplitude for our windows of interest. The source orientation was fixed to the dipole orientation with the highest strength.

Finally, the PAC analysis was performed on source level (i.e., virtual channels), for which the source space was subdivided into 22 anatomically defined brain parcels, including the intraparietal sulci, superior parietal lobes, frontal eye fields, middle frontal gyri and the temporoparietal junction (Wallis et al., 2015). Sensor-level time-series data were multiplied by spatial filters (constructed using LCMV beamformer) in order to obtain the time-resolved activity in each virtual channel.

268 **2.11 Multivariate pattern analysis**

269 To investigate how oscillatory dynamics influence the information content of neural activity, we
270 were interested in decoding two task features: (1) informative cue instruction (attend orientation
271 or spatial frequency), and (2) sample (i.e., the first grating) properties (orientation: clockwise or
272 counterclockwise; spatial frequency: low or high). For all multivariate pattern analysis (MVPA),
273 we used MNE Python (Gramfort et al., 2013) and Scikit-learn (Pedregosa et al., 2011). We
274 implemented a 4-fold cross-validation procedure within each participant. For each timepoint, we
275 trained a logistic regression classifier (L2-regularized) on three folds and tested on the left-out
276 fold. The analysis was shifted over time on a sample-by-sample basis. The input signal was the
277 broadband signal lowpass filtered at 35 Hz (Gwilliams & King, 2020; King et al., 2016). We
278 operationalized the decoding accuracy as area under the curve (AUC) by evaluating the similarity
279 between the true label categories of the test set and the probabilistic class labels (normalized
280 distance from the fit hyperplane: "predict_proba" in scikit-learn) of the same trials. We computed
281 the AUC under the null hypothesis by randomly shuffling the label categories and obtained a p-
282 value as the proportion of the null AUC estimates that exceeded the true AUC (evaluated at alpha
283 = 0.05).

284 We aimed to first demonstrate the decodability of the aforementioned features from the
285 broadband time-domain signal. We used trials from all conditions and tested decoding accuracy
286 against chance level (i.e., AUC = 0.5 for binary classification) using nonparametric cluster-based
287 permutation analysis (as described above). All task features could be decoded from the MEG
288 signal: informative cue instruction (attend to frequency or orientation), grating orientation
289 (clockwise or counterclockwise) and spatial frequency (low or high). For cue identity, group-level

290 decoding performance peaked around 150 ms after the onset of the first/second cue for the pre-
291 /retro-cue conditions, respectively (Figure 3AB), while for grating properties, group-level
292 decoding performance (for orientation and spatial frequency) peaked around 100 ms (Figure
293 3CD). It is important to note that the decodability of the grating features correlated negatively
294 with reaction times ($r = -0.5$, $p < 0.006$) and positively with accuracy ($r = 0.3$, $p = 0.042$). This
295 provides evidence that the decoded information reflects internal representation that are
296 behaviorally relevant (Ritchie et al., 2019).
297 Next, we asked whether oscillatory state shapes neural stimulus representations as reflected by
298 decoding performance. To test this, we evaluated how decoder accuracy was related to trial-by-
299 trial fluctuations of prestimulus power. We used the classification procedure explained above,
300 replacing the k-fold cross validation with a leave-one-out cross-validation (LOOCV) procedure. In
301 LOOCV, the classifier is fit to all trials but one, evaluating model performance on the remaining
302 "left-out" trial as a single-item test set. This is advantageous because: (1) it allows a maximal
303 amount of data to be used for training, thus reducing noise in the model fit; (2) it provides an
304 unbiased single-trial decoding estimate, which can be analyzed by a binning approach. For each
305 timepoint and test trial, we computed the probabilistic estimates of the logistic regression for
306 our feature of interest (cue information) and then grouped these results into five bins relative to
307 occipital sensor theta, alpha and beta power. Afterwards, for each frequency band separately,
308 the time-resolved AUC signal was contrasted between the bins of lowest and highest power using
309 nonparametric cluster-based permutation analysis.
310 Finally, to investigate the evolution of sample representations, we utilized the temporal
311 generalization method (King & Dehaene, 2014). For this analysis, each classifier was trained on

312 time *T* and tested on its ability to predict a given trial at time *T′*. This method estimates the
313 similarity of the coding pattern at T and *T′,* and thus the stability of the neural representation. In
314 order to facilitate the interpretation of our results, we averaged the AUC for training times within
315 the first 0.3 s following the sample onset. This was done separately for each bin and each band,
316 followed by contrasting the averaged temporal generalization matrices between the bins of
317 lowest and highest power using nonparametric cluster-based permutation analysis.

318 **2.12 Data and code availability**

319 All data and code used for stimulus presentation and analysis are available online at the
320 Donders Repository at https://doi.org/10.34973/tqy5-mh37.

321

# 3 Results

## 3.1 Behavioral results

In order to test our framework, we recorded MEG data from 33 healthy participants who performed a delayed match-to-sample working-memory paradigm where they evaluated orientation or spatial frequency of two visual gratings. The to-be-matched feature was indicated by a visual cue occurring either before (pre-cue) or after (retro-cue) sample presentation.

Overall, participants were faster matching the orientation than the spatial frequency of the gratings ($F(1,32) = 11.2$, $p = 0.001$; Figure 1B). There was no significant difference in RT between cue conditions ($F(1,32) = 2.7$, $p = 0.07$), nor a significant interaction between feature and cue conditions ($F(1,128) = 12.7$, $p = 0.66$). In terms of accuracy, participants were better at matching spatial frequency than orientation ($F(1,128) = 13.4$, $p < 0.001$; Figure 1C). There was no significant difference in accuracy between cue conditions ($F(1,128) = 2.7$, $p = 0.10$), though there was a significant interaction between the cue and feature conditions ($F(1,128) = 12.7$, $p < 0.001$): when matching the orientation of gratings, participants were better in the pre-cue than the retro-cue condition ($t(32) = -3.7$, $p < 0.001$), whereas when matching the spatial frequency of gratings, participants performed similarly in both cue conditions ($t(32) = 1.35$, $p = 0.17$).

Note that the absence of main cue effects demonstrates that task difficulty (performance) was comparable across our conditions of interest (i.e., pre- and retro-cue) and therefore does not constitute a confound in our subsequent analyses. Furthermore, accuracy linearly decreased with increasing RT ($R^2 = 0.21$, $p < 0.001$; Figure 1D), suggesting no speed-accuracy tradeoff.

342 **3.2 Impact of cueing on oscillatory dynamics**

343 In order to establish the proposed low-level mechanisms, we first investigated the differential
344 impacts of pre- and retro-cueing on oscillatory delta-to-theta phase, alpha power, and beta
345 power. The critical difference between the pre- and retro-cue conditions is the time when
346 participants are informed about the task-(ir)relevant feature. If alpha/beta decrease is critical for
347 the inhibition of task-irrelevant features, we expect alpha/beta power decrease to be contingent
348 upon the informative cues, after which selection (i.e., inhibition of the task-irrelevant feature
349 and/or enhancement of the relevant one) is possible. Similarly, if delta-to-theta phase plays a
350 role in input sampling, we would expect an increase in phase alignment following the informative
351 cues.

352 Indeed, we found significant differences between pre- and retro-cue conditions for all our
353 frequency bands of interest (Figure 4). Following the first cue, alpha and beta power decrease
354 was stronger for the pre-cue condition (in which the first cue was informative) in comparison to
355 the retro-cue condition (Figure 4CD; cluster-based permutation test, $p = 0.002$ and 0.003; $t = 0.35$
356 to 1 s and 0.34 to 0.77 s; centered on occipitoparietal and temporal sensors). Differences
357 between pre- and retro-cue conditions were mainly localized to left and right occipital cortices,
358 and right middle and superior temporal gyri.

359 This pattern was reversed following the second cue, with alpha and beta power decrease being
360 stronger for the retro-cue condition (in which the second cue was informative) in comparison to
361 the pre-cue condition (Figure 4CD; $p = 0.001$; $t = 3$ to 4 s and 2.6 to 3.6 s; centered on
362 occipitoparietal sensors). In addition, beta power decrease was stronger for the pre-cue vs. retro-
363 cue condition just prior to the probe presentation (Figure 4D; $p = 0.004$; $t = 3.8$ to 4.4 s; centered

364 on occipital sensors). Differences between pre- and retro-cue conditions were mainly localized
365 to left and right occipital cortices and the precentral gyrus, with beta effects extending more
366 towards the dorsolateral prefrontal cortex.
367 Furthermore, following the second cue, delta-to-theta inter-trial phase coherence was stronger
368 for the retro-cue condition in comparison to the pre-cue condition (Figure 4B; $p = 0.001$; $t = 3.6$
369 to 4.1 s; centered on occipital, parietal and temporal sensors). Differences between pre- and
370 retro-cue conditions were mainly localized to left and right occipital cortices, left inferior and
371 middle temporal gyrus, and left and right prefrontal cortices.
372 To summarize, the informative cue (i.e., the first cue on pre-cue trials and the second cue on
373 retro-cue trials) was followed by a stronger decrease in alpha and beta power, consistent with
374 the functional inhibition account. In addition, the informative cue on retro-cue trials was followed
375 by an increased phase alignment in the delta-to-theta band, consistent with a role in regulating
376 input sampling.

377 **3.3 Impact of oscillatory dynamics on behavioral performance**

378 Next, we asked whether any of the observed oscillatory dynamics impacted behavioral
379 performance. We expected that faster responses would coincide with (1) an increase in the phase
380 alignment of slow rhythms, reflecting their role in input sampling and temporal prediction, (2) a
381 decrease in occipital alpha/beta power, reflecting their gating role, and (3) increased phase-
382 amplitude coupling between slow and fast rhythms, reflecting the temporal coordination of fast
383 rhythms by slower ones. We binned trials into five bins based on RT and contrasted oscillatory
384 dynamics between bins of the slowest and fastest RT to test these predictions.

385 In line with our predictions, faster responses were associated with weaker alpha and beta power
386 before and during probe presentation (Figure 5CD; $p = 0.002$ and 0.001; $t = 4.1$ to 5.1 s; centered
387 on occipitoparietal sensors). These effects were localized to occipital cortices and the left inferior
388 and parietal cortices. Furthermore, faster responses were accompanied by an increase in ITC in
389 delta-to-theta frequencies (Figure 5B; $p < 0.001$; $t = 4.3$ to 5.5 s; across widespread sensors).
390 Differences were maximal in left and right post- and precentral gyri and lateral prefrontal
391 cortices.
392 We found that the coupling between the phase of 1–3 Hz oscillations and the amplitude of 30–
393 35 Hz oscillations was stronger for fast vs. slow RT in the intraparietal sulcus (Figure 6C; $p = 0.02$;
394 $t = 0$ to 5.5 s) and the superior parietal lobe (Figure 6D; $p = 0.07$; $t = 0$ to 3 s). Combined, these
395 results indicate that response speed was influenced by the phase alignment of delta-to-theta
396 oscillations as well as phase-amplitude coupling between slow and fast rhythms.
397 In sum, faster RT was preceded by (1) an increase in phase alignment and power of slow
398 oscillations, consistent with a role in regulating input sampling, (2) a prominent occipitoparietal
399 alpha/beta decrease, consistent with a gating-through-inhibition mechanism, and (3) an
400 increased phase-amplitude coupling between slow and fast oscillations, consistent with a role of
401 slow oscillations in temporal control of faster oscillations.

402 **3.4 Disentangling oscillatory dynamics from evoked responses**

403 To ensure that the ITC results (for the cueing and RT contrasts) did not stem from low-frequency
404 evoked (phase-locked) responses, we ran additional (control) analyses. For the cueing contrasts,
405 we compared ERFs between cue conditions and found that following the first cue, ERF amplitude
406 was higher for the pre-cue compared to the retro-cue (Figure 4A; $p < 0.001$; $t = 0.6$ to 1.1 s;

407 centered on centroparietal sensors). In addition, following the second cue, ERF amplitude was
408 higher for the retro-cue (Figure 4A; $p < 0.001$; t = 3.4 to 4.5 s; widespread). Further, we compared
409 the ERF and ITC differences between conditions at source level and found that ERF differences
410 were more prominent in right pre- and post-central gyri and prefrontal cortex (Figure 7A).
411 For the RT contrast, we compared ERFs between RT bins, and found that ERF amplitude was
412 higher for the fastest compared to the slowest RT bin (Figure 5A; $p < 0.001$; $p < 0.05$; t = 3.7 to
413 5.5 s; centered on occipitoparietal sensors). Further, we compared the ERF and ITC differences
414 between RT bins at source level and found that ERF differences were more prominent in left and
415 right pre- and post-central gyri and prefrontal cortex (Figure 7B). The significant differences
416 between the localization of the ERF and ITC effects suggest that these effects (ERF and ITC) might
417 reflect two separate phenomena.
418 Finally, we repeated the ITC analyses after subtraction of the evoked response from single-trial
419 data. The results were similar to those of our initial analysis: for the cueing contrast, in the retro-
420 cue condition, the presentation of the second cue was accompanied by an increase in ITC ($p <$
421 $0.001$; t = 3.5 to 4.3 s; widespread). For the RT contrast, faster responses were accompanied by
422 an increase in ITC ($p < 0.001$; t = 4.7 to 5.4 s; widespread). The persistence of effects after the
423 subtraction of evoked responses indicates that the low-frequency modulations cannot be fully
424 explained by evoked activity.

425 **3.5 Impact of oscillatory dynamics on decoding performance**

426 Finally, we investigated how oscillatory dynamics influence the information content of neural
427 activity patterns. We expected this content, indexed by classification accuracy, to be boosted by
428 a decrease in alpha power (i.e., release of inhibition) and an increase in beta power (reflecting

429 circuit recruitment). We trained neural classifiers to decode two task features: (1) informative
430 cue instruction (attend orientation or spatial frequency), and (2) grating properties (orientation:
431 clockwise or counterclockwise; spatial frequency: low or high).
432 Using a LOOCV procedure, we obtained unbiased single-trial responses of the classifiers. We then
433 grouped these single-trial estimates into five bins relative to occipital theta, alpha and beta
434 power, and contrasted the decoding accuracy between bins of the lowest and highest pre-cue
435 power. In accordance with our alpha predictions, we found significant differences contrasting
436 decoding accuracy between bins of low and high pre-stimulus occipital alpha power for pre-cue
437 instruction (Figure 8A; $p = 0.024$; $t = 0.2$ to $0.21$ and $0.47$ to $0.49$ s). In other words, decoding
438 accuracy was higher for cues that were preceded by low alpha power. No significant effects were
439 found for the decodability of retro-cue instruction by alpha power ($p = 0.37$).
440 In accordance with our beta predictions, we found significant differences contrasting decoding
441 accuracy between bins of low and high beta power for pre-cue instruction (Figure 8B; $p = 0.048$;
442 $t = 0.26$ to $0.27$ s). In addition, we found a trend contrasting decoding accuracy between bins of
443 low and high beta power for retro-cue instruction ($p = 0.057$; $t = 0.37$ to $0.39$ s). Thus, contrary
444 to alpha power, decoding accuracy was higher for cues that were preceded by high beta power.
445 No significant modulations were found for the decodability of pre- or retro-cue instruction by
446 theta power ($p > 0.5$ and $p = 0.21$, respectively), suggesting that this modulation of neural
447 stimulus information was specific to alpha and beta oscillations.
448 In order to further test our predictions regarding beta power and (reactivation of) information
449 content, we focused on decoding the spatial frequency and orientation of the sample stimulus.
450 To this end, we applied a time-generalization approach in which the classifier was trained at each

time point and tested on all other time points, thus allowing us to test the temporal stability of the information content. This approach yields a two-dimensional matrix across training and testing times. In order to reduce dimensionality, we averaged decoding accuracy across the early training time points (0 to 0.3 s post sample onset). We then contrasted the averaged decoding accuracy between the bins of lowest and highest pre-stimulus power.

In line with our predictions, we found significant differences between the averaged time-generalization matrices for decoding spatial frequency of the sample stimulus between bins of low and high occipital beta power (Figure 8C; $p = 0.022$). In other words, in trials where the sample was preceded by high beta power, classifiers trained on early time points more accurately decoded the sample's spatial frequency when tested on later time points (0.8 to 2.5 s) in comparison to trials preceded by low beta power. No significant effects were found for the decodability of the sample's orientation ($p = 0.47$) based on beta binning, though note that overall decoding performance was much lower for orientation than frequency (compare Figure 3 panels C and D for overall decoding performance along the diagonal).

No significant effects were found for the decodability of the sample's spatial frequency or orientation when binning was performed according to theta ($p = 0.11$ and $p = 0.2$, respectively) or alpha power ($p = 0.38$, $p = 0.46$), suggesting that the maintenance of neural stimulus information was specifically supported by beta oscillations.

In summary, alpha and beta oscillations differentially modulated the information content of neural activity. We found a negative relationship between alpha power and cue representations, as predicted by the inhibitory gating account, while we found a positive relationship between beta power and cue and sample representations, as predicted by the circuit recruitment account.

## 4 Discussion

In this study, we used a delayed match-to-sample working-memory task with pre- and retro-cueing in order to study a comprehensive framework that integrates the functional roles of specific neural oscillations, and, critically, the coordination between them. We directly tested our proposed framework in which slow rhythms sample task-relevant input, while alpha/beta gates the information flow by suppressing task-irrelevant processing, and beta further serves to recruit task-relevant circuits. Crucially, via phase-amplitude coupling, the timing of faster oscillations is controlled by slower rhythms. Indeed, in line with their role as a pace keeper of input sampling, we found that successful matching of probe and sample stimuli was preceded by an increased phase alignment that was confined to slow rhythms. As for the gate keeping role of alpha oscillations, we demonstrated a pattern of alpha decrease that temporally tracked the presentation of the informative cue, correlated with faster behavioral performance and increased neural information content (indexed by decoding performance). Importantly, we shed new light on the dual role of beta oscillations: on the one hand, an alpha-like inhibitory role, gating the processing of relevant input, and on the other hand, a circuit-activation role, relevant for (reactivation of) information maintenance.

### 4.1 Slow oscillations: the pace keeper

The first tenet of our framework is slow oscillations (1–6 Hz): we hypothesized that their phase regulates the sampling of task-relevant input and controls the timing of faster oscillations via phase-amplitude coupling. Indeed, we demonstrate that inter-trial coherence (i.e., phase alignment) of slow oscillations was more prominent after presentation of the informative cues, and was followed by faster responses. Interestingly, this effect occurred before probe onset and

496 was maximal in the pre- and post-central gyri and lateral prefrontal cortex. We also found that
497 on fast trials, the phase of slow oscillations was more strongly coupled to the amplitude of faster
498 oscillations (in the high beta range) in parietal areas.

499 We posit that this behavioral facilitation relies on more optimal temporal coordination reflected
500 in the phase adjustment of slow oscillations and their coupling to faster oscillations, which in turn
501 reflects better temporal prediction of probe onset. This is in line with previous reports that
502 temporal predictions are associated with improved behavioral performance (Coull & Nobre,
503 1998; Miniussi et al., 1999; Nobre et al., 2007) and increased phase alignment of slow oscillations
504 (Breska & Deouell, 2017), as well as recent evidence that the phase of slow oscillations predicts
505 behavioral performance (Herbst & Obleser, 2019). This finding further corroborates previous
506 reports of cross-frequency interactions during working memory (Bahramisharif et al., 2018;
507 Bastos et al., 2018; Berger et al., 2019) and adds to a growing number of studies demonstrating
508 the behavioral relevance of such coupling using intracranial (Axmacher et al., 2010) and scalp
509 (Puszta et al., 2020) EEG. Thus, temporal coordination by slow oscillations governs the sampling
510 of incoming stimuli (Busch et al., 2009; Fiebelkorn et al., 2013; Landau & Fries, 2012; VanRullen
511 et al., 2011) and controls the timing of faster oscillations.

512 Finally, in addition to these delta-to-theta dynamics, we found that faster behavioral
513 performance (and presentation of informative cues) cooccurred with stronger ERFs preceding
514 and following probe onset (i.e., contingent negative variation or CNV, and N1/P2 and P3,
515 respectively). This ERF enhancement may reflect better temporal prediction of probe onset in
516 fast trials, resulting in a more prominent anticipatory ramping up of neural activity (Bidet-Caulet
517 et al., 2015; Breska & Deouell, 2017; Brunia & van Boxtel, 2001). One potential concern is that

our spectral analysis picked up on this evoked activity (rather than genuine oscillatory dynamics). However, given that our phase results were not substantially altered by removing evoked activity and that delta-to-theta and ERF dynamics were not identically localized, we posit that these changes in evoked activity reflect an additional aspect of anticipatory mechanisms that are boosted by slow rhythm phase modulations, i.e., enhanced phase alignment leads to a stronger evoked response.

In summary, we outline how slow oscillations not only coordinate input sampling but also faster oscillatory dynamics for optimal information processing and subsequent performance. Future research should investigate how this endogenous rhythmic sampling mechanism is deployed in contexts of fixed versus varying temporal structure.

### 4.2 Alpha oscillations: the gate keeper of information processing

We found that decreases in alpha power actively track the presentation of informative cues; i.e., regardless of its position in time, the informative cue was followed by a more prominent decrease in occipitoparietal alpha power. Our results are in line with the proposed gating role for alpha oscillations: once an input has been sampled through slow oscillations, its subsequent processing depends on its task relevance, i.e., alpha oscillations up- and down-regulate cortical excitability in task-relevant and irrelevant networks, respectively (Jensen & Mazaheri, 2010; Klimesch et al., 2007). This regulation of cortical excitability has been shown to occur spontaneously (van Dijk et al., 2008; Iemi et al., 2021; Linkenkaer-Hansen et al., 2004; Samaha et al., 2017) or to track relevant input in space (ElShafei et al., 2018; Haegens et al., 2012; Mazaheri et al., 2014; Thut et al., 2006) or, as in the case of the current study, in time (Hanslmayr et al., 2011; Rohenkohl & Nobre, 2011; van Diepen et al., 2015; van Ede et al., 2017).

In addition, we found that faster responses were preceded by more prominent occipitoparietal alpha power decrease. This is in line with previous studies demonstrating that behavioral performance correlates negatively with alpha activity in task-relevant (Jiang et al., 2015; van Ede et al., 2017) and positively in task-irrelevant regions (Haegens et al., 2010; Yu et al., 2017). Both lines of results reflect the same low-level gating mechanism deployed to allocate more resources to task-relevant networks, either by directly boosting the processing of task-relevant information or by suppressing that of task-irrelevant information (i.e., distracting or competing stimuli).

Importantly, we demonstrate that pre-stimulus alpha power decrease enhances neural decodability (i.e., sensory representations) of subsequent task-relevant items. These results are in line with previous work reporting a negative relationship between decoding performance and pre-stimulus alpha power (Barne et al., 2020; van Ede et al., 2018), and shows how alpha through regulating cortical excitability might influence sensory representations.

### 4.3 Beta oscillations: a dual role in information gating and circuit formation

We hypothesized that multiple beta mechanisms exist, with one beta mechanism playing a local functionally inhibitory role ("inhibitory beta"), similar to alpha, and another beta mechanism allowing top-down flexible activation of task-relevant circuits that maintain the information required to successfully perform the task at hand ("circuit beta"). These two mechanisms translate to opposite power modulations.

In support for its inhibitory role, we show that similarly to alpha, decreases in prefrontal and occipitoparietal beta power are contingent upon the occurrence of the informative cue, and associated with faster responses. This is in line with previous reports on the alpha-like gating role played by beta oscillations (Bastos et al., 2018; van Ede et al., 2011; Miller et al., 2018).

562 Interestingly, while there is overlap in functionality and temporal patterns between alpha and
563 beta, the localization of the inhibitory beta effects extends more towards frontoparietal regions,
564 relative to that of the alpha effects.

565 In support for its circuit role, we demonstrate that increases (rather than decreases) in beta
566 power index a stronger decoding and maintenance of task-relevant features, i.e., the decodability
567 of stimuli preceded by high beta power was boosted and generalized for longer durations. This is
568 in line with previous studies demonstrating that beta power correlates with stimulus information
569 maintained in working memory as well as subsequent decision outcomes (Haegens et al., 2017;
570 Proskovec et al., 2019; von Lautz et al., 2017). Here we go one step further, by directly linking the
571 power of beta oscillations to the quality of information content in neural activity patterns. We
572 posit that stronger beta synchronization indexes a stronger (longer lasting) setting up of task-
573 relevant circuits (i.e., working-memory nodes). In turn, this enhanced circuit recruitment leads
574 to more efficient maintenance of stimulus features and thus allows them to be decoded for
575 longer durations.

576 Taken together, our results corroborate the proposed dual roles for beta rhythms in our
577 framework (Miller et al., 2018; Spitzer & Haegens, 2017). Future invasive studies are required to
578 dissociate the underlying generators (e.g., on the cell circuit/laminar level) of these proposed
579 dual betas. In addition, the temporal and spatial evolution of alpha and beta rhythms should be
580 thoroughly compared, in order to highlight potential differences and similarities in their roles in
581 active inhibition.

### 4.4 Conclusion

In summary, we demonstrate how rhythms from the delta to beta range might subserve higher-level cognitive functions by providing low-level mechanistic operations. Combined, these oscillatory building blocks allow for selective sampling of input, disengaging and engaging task-irrelevant and relevant networks, and temporal organization of these respective dynamics. Critically, we find that these oscillatory dynamics correlate both with the behavioral performance of the participant, and with the information content in the recorded brain signal.

## References


Axmacher, N., Henseler, M. M., Jensen, O., Weinreich, I., Elger, C. E., & Fell, J. (2010). Cross-frequency coupling supports multi-item working memory in the human hippocampus. *Proceedings of the National Academy of Sciences*, *107*(7), 3228–3233. https://doi.org/10.1073/pnas.0911531107

Bahmani, Z., Daliri, M. R., Merrikhi, Y., Clark, K., & Noudoost, B. (2018). Working Memory Enhances Cortical Representations via Spatially Specific Coordination of Spike Times. *Neuron*, *97*(4), 967-979.e6. https://doi.org/10.1016/j.neuron.2018.01.012

Bahramisharif, A., Jensen, O., Jacobs, J., & Lisman, J. (2018). Serial representation of items during working memory maintenance at letter-selective cortical sites. *PLOS Biology*, *16*(8), e2003805. https://doi.org/10.1371/journal.pbio.2003805

Barne, L. C., de Lange, F. P., & Cravo, A. M. (2020). Prestimulus alpha power is related to the strength of stimulus representation. *Cortex*, *132*, 250–257. https://doi.org/10.1016/j.cortex.2020.08.017

Bastos, A. M., Loonis, R., Kornblith, S., Lundqvist, M., & Miller, E. K. (2018). Laminar recordings in frontal cortex suggest distinct layers for maintenance and control of working memory. *Proceedings of the National Academy of Sciences*, *115*(5), 1117–1122. https://doi.org/10.1073/pnas.1710323115

Bates, D., Mächler, M., Bolker, B., & Walker, S. (2015). Fitting Linear Mixed-Effects Models Using lme4. *Journal of Statistical Software*, *67*(1), 1–48. https://doi.org/10.18637/jss.v067.i01

Berger, B., Griesmayr, B., Minarik, T., Biel, A. L., Pinal, D., Sterr, A., & Sauseng, P. (2019). Dynamic regulation of interregional cortical communication by slow brain oscillations during working memory. *Nature Communications*, *10*(1), 4242. https://doi.org/10.1038/s41467-019-12057-0

Bidet-Caulet, A., Bottemanne, L., Fonteneau, C., Giard, M.-H., & Bertrand, O. (2015). Brain Dynamics of Distractibility: Interaction Between Top-Down and Bottom-Up Mechanisms of Auditory Attention. *Brain Topography*, *28*(3), 423–436. https://doi.org/10.1007/s10548-014-0354-x

Bishop, G. H. (1932). Cyclic changes in excitability of the optic pathway of the rabbit. *American Journal of Physiology*, *103*(1), 213–224.

Brainard, D. H. (1997). The Psychophysics Toolbox. *Spatial Vision*, *10*(4), 433–436. https://doi.org/10.1163/156856897X00357

Breska, A., & Deouell, L. Y. (2017). Neural mechanisms of rhythm-based temporal prediction: Delta phase-locking reflects temporal predictability but not rhythmic entrainment. *PLoS Biology*, *15*(2), e2001665.

Brunia, C. H., & van Boxtel, G. J. (2001). Wait and see. *International Journal of Psychophysiology*, *43*(1), 59–75. https://doi.org/10.1016/S0167-8760(01)00179-9

Busch, N. A., Dubois, J., & VanRullen, R. (2009). The Phase of Ongoing EEG Oscillations Predicts Visual Perception. *The Journal of Neuroscience*, *29*(24), 7869–7876. https://doi.org/10.1523/jneurosci.0113-09.2009

Buschman, T. J., & Miller, E. K. (2007). Top-Down Versus Bottom-Up Control of Attention in the Prefrontal and Posterior Parietal Cortices. *Science*, *Ci*, 8–11.

Buzsaki, G. (2006). *Rhythms of the Brain*. Oxford University Press.

Canolty, R. T., Ganguly, K., Kennerley, S. W., Cadieu, C. F., Koepsell, K., Wallis, J. D., & Carmena, J. M. (2010). Oscillatory phase coupling coordinates anatomically dispersed functional cell assemblies. *Proceedings of the National Academy of Sciences*, *107*(40), 17356–17361. https://doi.org/10.1073/pnas.1008306107

Combrisson, E., Nest, T., Brovelli, A., Ince, R. A. A., Soto, J. L. P., Guillot, A., & Jerbi, K. (2020). Tensorpac: An open-source Python toolbox for tensor-based phase-amplitude coupling measurement in electrophysiological brain signals. *PLOS Computational Biology*, *16*(10), e1008302. https://doi.org/10.1371/journal.pcbi.1008302

Coull, J. T., & Nobre, A. C. (1998). Where and when to pay attention: The neural systems for directing attention to spatial locations and to time intervals as revealed by both PET and fMRI. *Journal of Neuroscience*, *18*(18), 7426–7435.

Dijk, H. van, Schoffelen, J.-M., Oostenveld, R., & Jensen, O. (2008). Prestimulus Oscillatory Activity in the Alpha Band Predicts Visual Discrimination Ability. *Journal of Neuroscience*, *28*(8), 1816–1823. https://doi.org/10.1523/JNEUROSCI.1853-07.2008

Dugué, L., Marque, P., & VanRullen, R. (2015). Theta Oscillations Modulate Attentional Search Performance Periodically. *Journal of Cognitive Neuroscience*, *27*(5), 945–958. https://doi.org/10.1162/jocn_a_00755

Ede, F. van, Lange, F. de, Jensen, O., & Maris, E. (2011). Orienting Attention to an Upcoming Tactile Event Involves a Spatially and Temporally Specific Modulation of Sensorimotor Alpha- and Beta-Band Oscillations. *Journal of Neuroscience*, *31*(6), 2016–2024. https://doi.org/10.1523/JNEUROSCI.5630-10.2011

ElShafei, H. A., Bouet, R., Bertrand, O., & Bidet-Caulet, A. (2018). Two Sides of the Same Coin: Distinct Sub-Bands in the Alpha Rhythm Reflect Facilitation and Suppression Mechanisms during Auditory Anticipatory Attention. *Eneuro*, ENEURO.0141-18.2018. https://doi.org/10.1523/ENEURO.0141-18.2018

Engel, A. K., & Fries, P. (2010). Beta-band oscillations—Signalling the status quo? *Current Opinion in Neurobiology*, *20*(2), 156–165. https://doi.org/10.1016/j.conb.2010.02.015

Fiebelkorn, I. C., & Kastner, S. (2019). A rhythmic theory of attention. *Trends in Cognitive Sciences*, *23*(2), 87–101.

Fiebelkorn, I. C., Saalmann, Y. B., & Kastner, S. (2013). Rhythmic sampling within and between objects despite sustained attention at a cued location. *Current Biology*, *23*(24), 2553–2558.

Gramfort, A., Luessi, M., Larson, E., Engemann, D., Strohmeier, D., Brodbeck, C., Goj, R., Jas, M., Brooks, T., Parkkonen, L., & Hämäläinen, M. (2013). MEG and EEG data analysis with MNE-Python. *Frontiers in Neuroscience*, *7*, 267. https://doi.org/10.3389/fnins.2013.00267

Griffiths, B. J., Mayhew, S. D., Mullinger, K. J., Jorge, J., Charest, I., Wimber, M., & Hanslmayr, S. (2019). Alpha/beta power decreases track the fidelity of stimulus-specific information. *ELife*, *8*, e49562. https://doi.org/10.7554/eLife.49562

Gross, J., Kujala, J., Hämäläinen, M., Timmermann, L., Schnitzler, A., & Salmelin, R. (2001). Dynamic imaging of coherent sources: Studying neural interactions in the human brain. *Proceedings of the National Academy of Sciences*, *98*(2), 694–699.

Gwilliams, L., & King, J.-R. (2020). Recurrent processes support a cascade of hierarchical decisions. *ELife*, *9*, e56603. https://doi.org/10.7554/eLife.56603

Haegens, S., Cousijn, H., Wallis, G., Harrison, P. J., & Nobre, A. C. (2014). Inter- and intra-individual variability in alpha peak frequency. *NeuroImage*, *92*, 46–55. https://doi.org/10.1016/j.neuroimage.2014.01.049

Haegens, S., Luther, L., & Jensen, O. (2012). Somatosensory Anticipatory Alpha Activity Increases to Suppress Distracting Input. *Journal of Cognitive Neuroscience*, *24*(3), 677–685. https://doi.org/10.1162/jocn_a_00164

Haegens, S., Osipova, D., Oostenveld, R., & Jensen, O. (2010). Somatosensory working memory performance in humans depends on both engagement and disengagement of regions in a distributed network. *Human Brain Mapping*, *31*(1), 26–35. https://doi.org/10.1002/hbm.20842

Haegens, S., Vergara, J., Rossi-Pool, R., Lemus, L., & Romo, R. (2017). Beta oscillations reflect supramodal information during perceptual judgment. *Proceedings of the National Academy of Sciences*, *114*(52), 13810–13815. https://doi.org/10.1073/pnas.1714633115

Hanslmayr, S., Gross, J., Klimesch, W., & Shapiro, K. L. (2011). The role of α oscillations in temporal attention. *Brain Research Reviews*, *67*(1–2), 331–343. https://doi.org/10.1016/j.brainresrev.2011.04.002

Helfrich, R. F., Breska, A., & Knight, R. T. (2019). Neural entrainment and network resonance in support of top-down guided attention. *Current Opinion in Psychology*, *29*, 82–89. https://doi.org/10.1016/j.copsyc.2018.12.016

Henry, M. J., Herrmann, B., & Obleser, J. (2016). Neural Microstates Govern Perception of Auditory Input without Rhythmic Structure. *The Journal of Neuroscience: The Official Journal of the Society for Neuroscience*, *36*(3), 860–871. https://doi.org/10.1523/JNEUROSCI.2191-15.2016

Herbst, S. K., & Landau, A. N. (2016). Rhythms for cognition: The case of temporal processing. *Current Opinion in Behavioral Sciences*, *8*, 85–93. https://doi.org/10.1016/j.cobeha.2016.01.014

Herbst, S. K., & Obleser, J. (2019). Implicit temporal predictability enhances pitch discrimination sensitivity and biases the phase of delta oscillations in auditory cortex. *NeuroImage*, *203*, 116198. https://doi.org/10.1016/j.neuroimage.2019.116198

Herding, J., Spitzer, B., & Blankenburg, F. (2016). Upper Beta Band Oscillations in Human Premotor Cortex Encode Subjective Choices in a Vibrotactile Comparison Task. *Journal of Cognitive Neuroscience*, *28*(5), 668–679. https://doi.org/10.1162/jocn_a_00932

Iemi, L., Gwilliams, L., Samaha, J., Auksztulewicz, R., Cycowicz, Y. M., King, J.-R., Nikulin, V. V., Thesen, T., Doyle, W., Devinsky, O., Schroeder, C. E., Melloni, L., & Haegens, S. (2021).

*Spontaneous neural oscillations influence behavior and sensory representations by suppressing neuronal excitability* [Preprint]. Neuroscience. https://doi.org/10.1101/2021.03.01.433450

Jensen, O., & Mazaheri, A. (2010). Shaping functional architecture by oscillatory alpha activity: Gating by inhibition. *Frontiers in Human Neuroscience*, *4*, 186. https://doi.org/10.3389/fnhum.2010.00186

Jiang, H., van Gerven, M. A. J., & Jensen, O. (2015). Modality-specific alpha modulations facilitate long-term memory encoding in the presence of distracters. *Journal of Cognitive Neuroscience*, *27*(3), 583–592. https://doi.org/10.1162/jocn_a_00726

Jung, T.-P., Makeig, S., McKeown, M. J., Bell, A. J., Lee, T.-W., & Sejnowski, T. J. (2001). Imaging Brain Dynamics Using Independent Component Analysis. *Proceedings of the IEEE. Institute of Electrical and Electronics Engineers*, *89*(7), 1107–1122. https://doi.org/10.1109/5.939827

Kayser, S. J., McNair, S. W., & Kayser, C. (2016). Prestimulus influences on auditory perception from sensory representations and decision processes. *Proceedings of the National Academy of Sciences of the United States of America*, *113*(17), 4842–4847. https://doi.org/10.1073/pnas.1524087113

King, J.-R., & Dehaene, S. (2014). Characterizing the dynamics of mental representations: The temporal generalization method. *Trends in Cognitive Sciences*, *18*(4), 203–210. https://doi.org/10.1016/j.tics.2014.01.002

King, J.-R., Pescetelli, N., & Dehaene, S. (2016). Brain Mechanisms Underlying the Brief Maintenance of Seen and Unseen Sensory Information. *Neuron*, *92*(5), 1122–1134. https://doi.org/10.1016/j.neuron.2016.10.051

Klimesch, W., Sauseng, P., & Hanslmayr, S. (2007). Jensen and Mazaheri. *Brain Research Reviews*, *53*(1), 63–88. https://doi.org/10.1016/J.BRAINRESREV.2006.06.003

Landau, A. N., & Fries, P. (2012). Attention Samples Stimuli Rhythmically. *Current Biology*, *22*(11), 1000–1004. https://doi.org/10.1016/j.cub.2012.03.054

Linkenkaer-Hansen, K., Nikulin, V. V., Palva, S., Ilmoniemi, R. J., & Palva, J. M. (2004). Prestimulus Oscillations Enhance Psychophysical Performance in Humans. *Journal of Neuroscience*, *24*(45), 10186–10190. https://doi.org/10.1523/JNEUROSCI.2584-04.2004

Lundqvist, M., Rose, J., Herman, P., Brincat, S. L., Buschman, T. J., & Miller, E. K. (2016). Gamma and Beta Bursts Underlie Working Memory. *Neuron*, *90*(1), 152–164. https://doi.org/10.1016/j.neuron.2016.02.028

Maris, E., & Oostenveld, R. (2007). Nonparametric statistical testing of EEG- and MEG-data. *Journal of Neuroscience Methods*, *164*(1), 177–190. https://doi.org/10.1016/j.jneumeth.2007.03.024

Mazaheri, A., van Schouwenburg, M. R., Dimitrijevic, A., Denys, D., Cools, R., & Jensen, O. (2014). Region-specific modulations in oscillatory alpha activity serve to facilitate processing in the visual and auditory modalities. *NeuroImage*, *87*, 356–362. https://doi.org/10.1016/j.neuroimage.2013.10.052

Meij, R. van der, Kahana, M., & Maris, E. (2012). Phase–Amplitude Coupling in Human Electrocorticography Is Spatially Distributed and Phase Diverse. *Journal of Neuroscience*, *32*(1), 111–123. https://doi.org/10.1523/JNEUROSCI.4816-11.2012

Miller, E. K., Lundqvist, M., & Bastos, A. M. (2018). Working Memory 2.0. *Neuron*, *100*(2), 463–475. https://doi.org/10.1016/j.neuron.2018.09.023

Miniussi, C., Wilding, E. L., Coull, J. T., & Nobre, A. C. (1999). Orienting attention in time. Modulation of brain potentials. *Brain: A Journal of Neurology*, *122 ( Pt 8)*, 1507–1518. https://doi.org/10.1093/brain/122.8.1507

Mitra, P. P., & Pesaran, B. (1999). Analysis of dynamic brain imaging data. *Biophysical Journal*, *76*(2), 691–708. https://doi.org/10.1016/S0006-3495(99)77236-X

Nobre, A., Correa, A., & Coull, J. (2007). The hazards of time. *Current Opinion in Neurobiology*, *17*(4), 465–470. https://doi.org/10.1016/j.conb.2007.07.006

Nolte, G. (2003). The magnetic lead field theorem in the quasi-static approximation and its use for magnetoencephalography forward calculation in realistic volume conductors. *Physics in Medicine and Biology*, *48*(22), 3637–3652. https://doi.org/10.1088/0031-9155/48/22/002

Oostenveld, R., Fries, P., Maris, E., & Schoffelen, J.-M. (2011). FieldTrip: Open source software for advanced analysis of MEG, EEG, and invasive electrophysiological data. *Computational Intelligence and Neuroscience*, *2011*, 156869. https://doi.org/10.1155/2011/156869

Pedregosa, F., Varoquaux, G., Gramfort, A., Michel, V., Thirion, B., Grisel, O., Blondel, M., Prettenhofer, P., Weiss, R., & Dubourg, V. (2011). Scikit-learn: Machine learning in Python. *The Journal of Machine Learning Research*, *12*, 2825–2830.

Pfurtscheller, G., & Lopes da Silva, F. H. (1999). Event-related EEG/MEG synchronization and desynchronization: Basic principles. *Clinical Neurophysiology: Official Journal of the International Federation of Clinical Neurophysiology*, *110*(11), 1842–1857. https://doi.org/10.1016/s1388-2457(99)00141-8

Proskovec, A. L., Wiesman, A. I., Heinrichs-Graham, E., & Wilson, T. W. (2019). Load effects on spatial working memory performance are linked to distributed alpha and beta oscillations. *Human Brain Mapping*, *40*(12), 3682–3689. https://doi.org/10.1002/hbm.24625

Puszta, A., Pertich, Á., Giricz, Z., Nyujtó, D., Bodosi, B., Eördegh, G., & Nagy, A. (2020). Predicting Stimulus Modality and Working Memory Load During Visual- and Audiovisual-Acquired Equivalence Learning. *Frontiers in Human Neuroscience*, *14*, 410. https://doi.org/10.3389/fnhum.2020.569142

Ritchie, J. B., Kaplan, D. M., & Klein, C. (2019). Decoding the Brain: Neural Representation and the Limits of Multivariate Pattern Analysis in Cognitive Neuroscience. *The British Journal for the Philosophy of Science*, *70*(2), 581–607. https://doi.org/10.1093/bjps/axx023

Rohenkohl, G., & Nobre, A. C. (2011). Alpha oscillations related to anticipatory attention follow temporal expectations. *Journal of Neuroscience*, *31*(40), 14076–14084.

Salazar, R. F., Dotson, N. M., Bressler, S. L., & Gray, C. M. (2012). Content-specific fronto-parietal synchronization during visual working memory. *Science (New York, N.Y.)*, *338*(6110), 1097–1100. https://doi.org/10.1126/science.1224000

Samaha, J., Iemi, L., & Postle, B. R. (2017). Prestimulus alpha-band power biases visual discrimination confidence, but not accuracy. *Consciousness and Cognition*, *54*, 47–55. https://doi.org/10.1016/j.concog.2017.02.005

Sauseng, P., Peylo, C., Biel, A. L., Friedrich, E. V. C., & Romberg-Taylor, C. (2019). Does cross-frequency phase coupling of oscillatory brain activity contribute to a better understanding of visual working memory? *British Journal of Psychology*, *110*(2), 245–255. https://doi.org/10.1111/bjop.12340

Searle, S. R., Speed, F. M., & Milliken, G. A. (1980). Population marginal means in the linear model: An alternative to least squares means. *The American Statistician*, *34*(4), 216–221.

Singer, W. (1999). Neuronal synchrony: A versatile code for the definition of relations? *Neuron*, *24*(1), 49–65, 111–125. https://doi.org/10.1016/s0896-6273(00)80821-1

Spitzer, B., & Haegens, S. (2017). Beyond the Status Quo: A Role for Beta Oscillations in Endogenous Content (Re)Activation. *ENeuro*, *4*(4). https://doi.org/10.1523/ENEURO.0170-17.2017

Stolk, A., Todorovic, A., Schoffelen, J.-M., & Oostenveld, R. (2013). Online and offline tools for head movement compensation in MEG. *NeuroImage*, *68*, 39–48. https://doi.org/10.1016/j.neuroimage.2012.11.047

Tallon-Baudry, C., Bertrand, O., Delpuech, C., & Pernier, J. (1996). Stimulus Specificity of Phase-Locked and Non-Phase-Locked 40 Hz Visual Responses in Human. *Journal of Neuroscience*, *16*(13), 4240–4249. https://doi.org/10.1523/JNEUROSCI.16-13-04240.1996

Team, R. C. (2014). R: A Language and Environment for Statistical Computing. Vienna: R Foundation for Statistical Computing. Available online at: h ttp://.*w Www.R-Project. Org*.

Thut, G., Nietzel, A., Brandt, S. A., & Pascual-Leone, A. (2006). α-Band Electroencephalographic Activity over Occipital Cortex Indexes Visuospatial Attention Bias and Predicts Visual Target Detection. *Journal of Neuroscience*, *26*(37), 9494–9502. https://doi.org/10.1523/JNEUROSCI.0875-06.2006

van Diepen, R. M., Cohen, M. X., Denys, D., & Mazaheri, A. (2015). Attention and temporal expectations modulate power, not phase, of ongoing alpha oscillations. *Journal of Cognitive Neuroscience*, *27*(8), 1573–1586. https://doi.org/10.1162/jocn_a_00803

van Ede, F., Chekroud, S. R., Stokes, M. G., & Nobre, A. C. (2018). Decoding the influence of anticipatory states on visual perception in the presence of temporal distractors. *Nature Communications*, *9*(1), 1449. https://doi.org/10.1038/s41467-018-03960-z

van Ede, F., Niklaus, M., & Nobre, A. C. (2017). Temporal Expectations Guide Dynamic Prioritization in Visual Working Memory through Attenuated α Oscillations. *The Journal of Neuroscience*, *37*(2), 437–445. https://doi.org/10.1523/JNEUROSCI.2272-16.2016

Van Veen, B. D., van Drongelen, W., Yuchtman, M., & Suzuki, A. (1997). Localization of brain electrical activity via linearly constrained minimum variance spatial filtering. *Biomedical Engineering, IEEE Transactions On*, *44*(9), 867–880. https://doi.org/10.1109/10.623056

VanRullen, R. (2016). Perceptual cycles. *Trends in Cognitive Sciences*, *20*(10), 723–735.

VanRullen, R., Busch, N., Drewes, J., & Dubois, J. (2011). Ongoing EEG Phase as a Trial-by-Trial Predictor of Perceptual and Attentional Variability. *Frontiers in Psychology*, *2*, 60. https://doi.org/10.3389/fpsyg.2011.00060

Varela, F., Lachaux, J. P., Rodriguez, E., & Martinerie, J. (2001). The brainweb: Phase synchronization and large-scale integration. *Nature Reviews Neuroscience*, *2*(4), 229–239. https://doi.org/10.1038/35067550

von Lautz, A. H., Herding, J., Ludwig, S., Nierhaus, T., Maess, B., Villringer, A., & Blankenburg, F. (2017). Gamma and Beta Oscillations in Human MEG Encode the Contents of Vibrotactile Working Memory. *Frontiers in Human Neuroscience*, *11*, 576. https://doi.org/10.3389/fnhum.2017.00576

Wallis, G., Stokes, M., Cousijn, H., Woolrich, M., & Nobre, A. C. (2015). Frontoparietal and Cingulo-opercular Networks Play Dissociable Roles in Control of Working Memory. *Journal of Cognitive Neuroscience*, *27*(10), 2019–2034. https://doi.org/10.1162/jocn_a_00838

Wang, X.-J. (2010). Neurophysiological and computational principles of cortical rhythms in cognition. *Physiological Reviews*, *90*(3), 1195–1268. https://doi.org/10.1152/physrev.00035.2008

Yu, X., Chen, Y., Qiu, J., Li, X., & Huang, X. (2017). Neural oscillations associated with auditory duration maintenance in working memory. *Scientific Reports*, *7*(1), 5695. https://doi.org/10.1038/s41598-017-06078-2

Zion Golumbic, E. M., Ding, N., Bickel, S., Lakatos, P., Schevon, C. A., McKhann, G. M., Goodman, R. R., Emerson, R., Mehta, A. D., Simon, J. Z., Poeppel, D., & Schroeder, C. E. (2013). Mechanisms Underlying Selective Neuronal Tracking of Attended Speech at a 'Cocktail Party.' *Neuron*, *77*(5), 980–991. https://doi.org/10.1016/j.neuron.2012.12.037

862 **Legends**

863 **Figure 1. Paradigm and behavioral results.**

864 [A] Schematic of the four trial types: attend orientation (two solid lines) or attend frequency (two
865 dotted lines) for pre- and retro-cue conditions (first vs. second cue is informative; uninformative
866 cues consist of a solid and dotted line). [B] Participants were slower and [C] more accurate
867 matching the spatial frequency (gray bars) of the visual gratings compared to orientation
868 (orange). This effect was mainly driven by the pre-cue condition. Within each boxplot, the
869 horizontal line represents the median, the box delineates the area between the first and third
870 quartiles (interquartile range). [D] Average accuracy across RT bins. Error bars represent standard
871 error of the mean. ** $P < 0.01$, *** $P < 0.001$.

872 **Figure 2. Alpha and beta peak detection.**

873 [A] Grand-averaged ERF of sensors (highlighted in sensor space) displaying maximal post-grating
874 ERFs within 200 ms following the grating onset. Gray shaded area around the curve denotes
875 between-participants standard error. Light gray shaded box highlights the time period used to
876 select channels with maximal post-grating ERFs. [B] Power spectra (averaged over same sensors
877 marked in A; t = -1 to 0 s relative to first cue onset) showing alpha and beta peaks.

878 **Figure 3. Decodability of task features.**

879 [A] Temporal sample-by-sample decoding of cue features (attend frequency vs. attend
880 orientation) for pre- and [B] retro-cues. [C] Decoding performance for grating spatial frequency
881 (low vs. high) and [D] grating orientation (clockwise vs. counterclockwise). Gray bars indicate
882 significance of decoding accuracy (t-test vs. chance).

883 **Figure 4. Cue-related power modulations.**

[A] Grand average ERFs for the pre- (green) and retro-cue conditions (purple). Shaded areas denote between-participants standard error. Gray bars indicate significant differences between conditions. Topographies show statistical and power distributions of these significant differences in sensor and source space, respectively. [B] Inter-trial phase coherence (averaged between 1 and 6 Hz) for the pre- and retro-cue conditions. [C] Time course of oscillatory power averaged within the alpha band. [D] Same as C but for the beta band. For all time courses, all sensors displaying significant differences as highlighted by the topographies were included in the plot.

**Figure 5. Correlates of behavioral performance: power and phase.**

[A] Grand average ERFs (occipital sensors) for the slowest (red) and fastest RT bins (blue). Shaded areas denote between-participants standard error. Gray bars indicate significant differences between conditions. Topographies show statistical and power distributions of these significant differences in sensor and source space, respectively. [B] Time course of inter-trial phase coherence (averaged between 1 and 6Hz) for the slowest and fastest RT bins. [C] Time course of oscillatory power averaged within the alpha band. Dashed lines represent mean power (i.e., normalized power = 1). [D] Same as C but for the beta band.

**Figure 6. Correlates of behavioral performance: ITC and PAC.**

[A] TFR of statistical differences in PAC between the slowest and fastest RT bins (masked at $p < 0.05$) in the intraparietal sulcus (as highlighted in green on brain surface). Negative values (blue) indicate higher PAC for the fastest RT bin. [B] Same as A for the superior parietal lobe.

**Figure 7. Correlates of behavioral performance: ERFs.**

904 [A] Source level topographies of the statistical differences between ERF and ITC for the cueing
905 contrast (pre- versus retro-cue; t=3.6 to 4.1 s; masked at $p < 0.05$). [B] Same as A for the RT
906 contrast (slow versus fast RT bin; t= 4.4 to 5.1 s).

907 **Figure 8. Effects of pre-stimulus oscillatory power on decodability**.

908 [A] Temporal sample-by-sample decoding of pre-cue (left panel) and retro-cue (right panel)
909 instruction for the bins of lowest and highest occipital alpha power preceding cue onset. [B] Same
910 as A for the beta band. [C] Averaged time-generalization matrices (over the first 0.3 s of training
911 time) of decoding the sample's orientation (left panel) and frequency (right panel) for the bins of
912 lowest and highest beta power preceding sample onset. Gray bars indicate significant differences
913 between low and high power bins.

914

## Figures

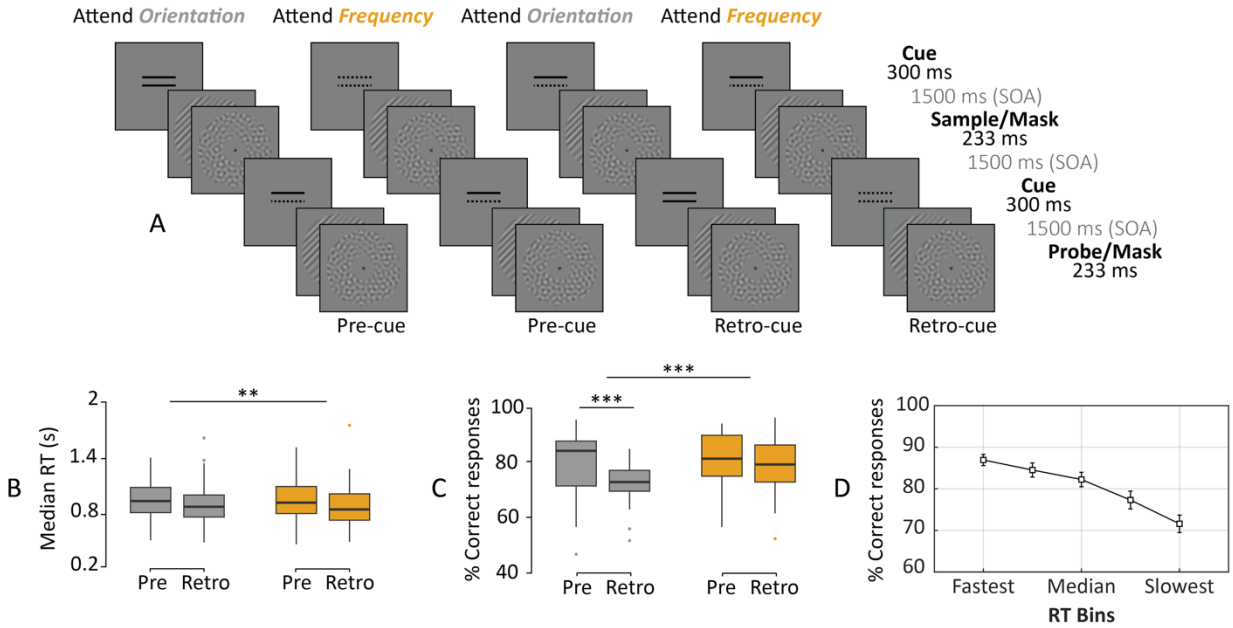


**Figure 1**

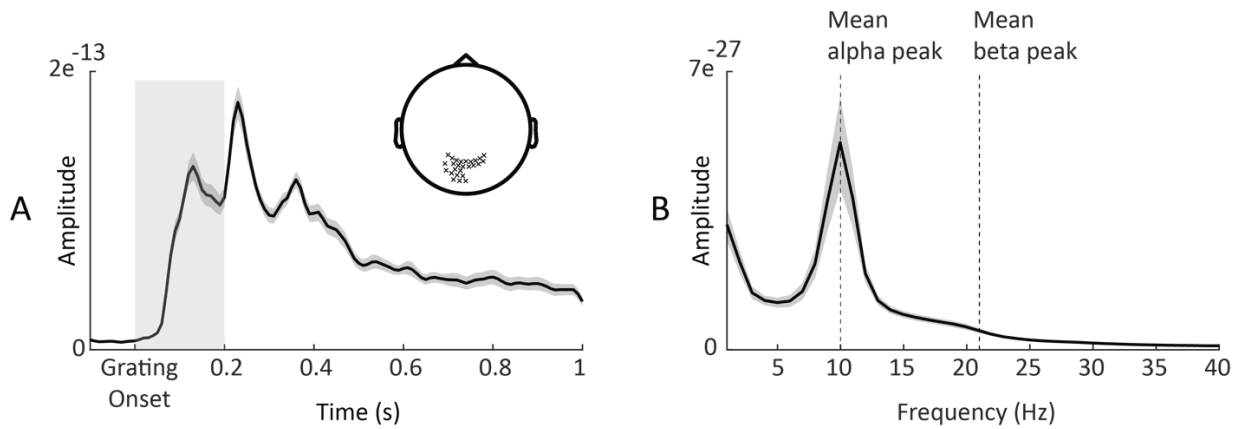


**Figure 2**

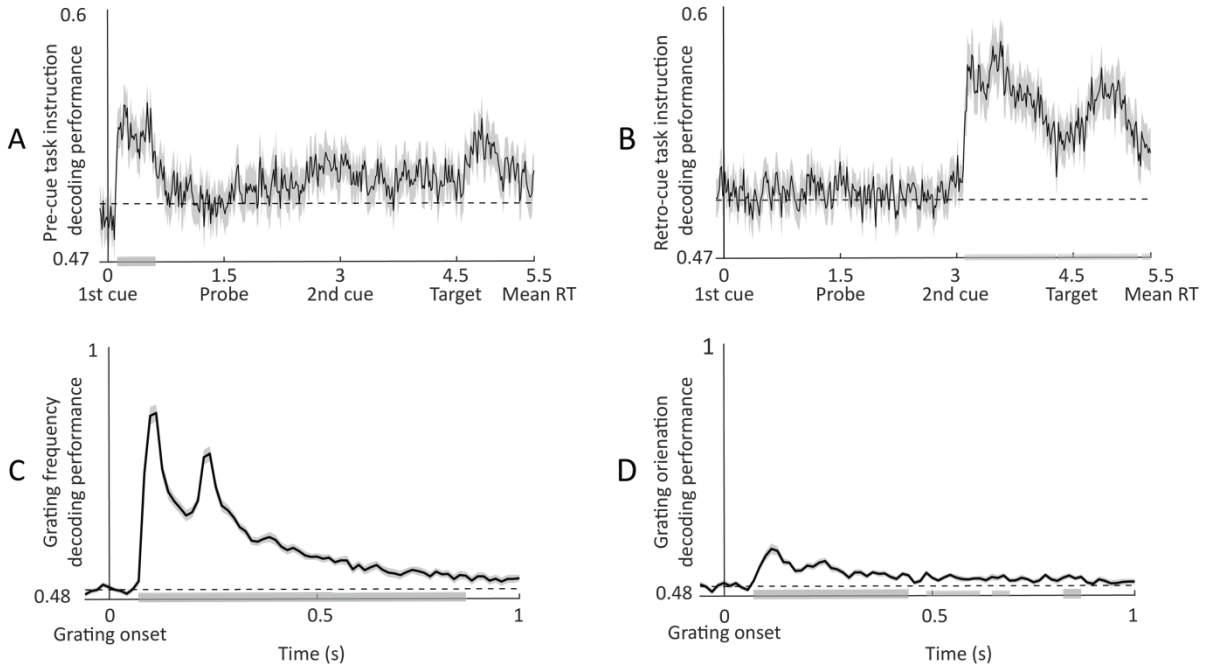
A
Pre-cue task instruction decoding performance
0.6
0.47
0
1.5
3
4.5
5.5
1st cue
Probe
2nd cue
Target
Mean RT
B
Retro-cue task instruction decoding performance
0.6
0.47
0
1.5
3
4.5
5.5
1st cue
Probe
2nd cue
Target
Mean RT
C
Grating frequency decoding performance
1
0.48
0
0.5
1
Grating onset
Time (s)
D
Grating orienation decoding performance
1
0.48
0
0.5
1
Grating onset
Time (s)

**Figure 3**

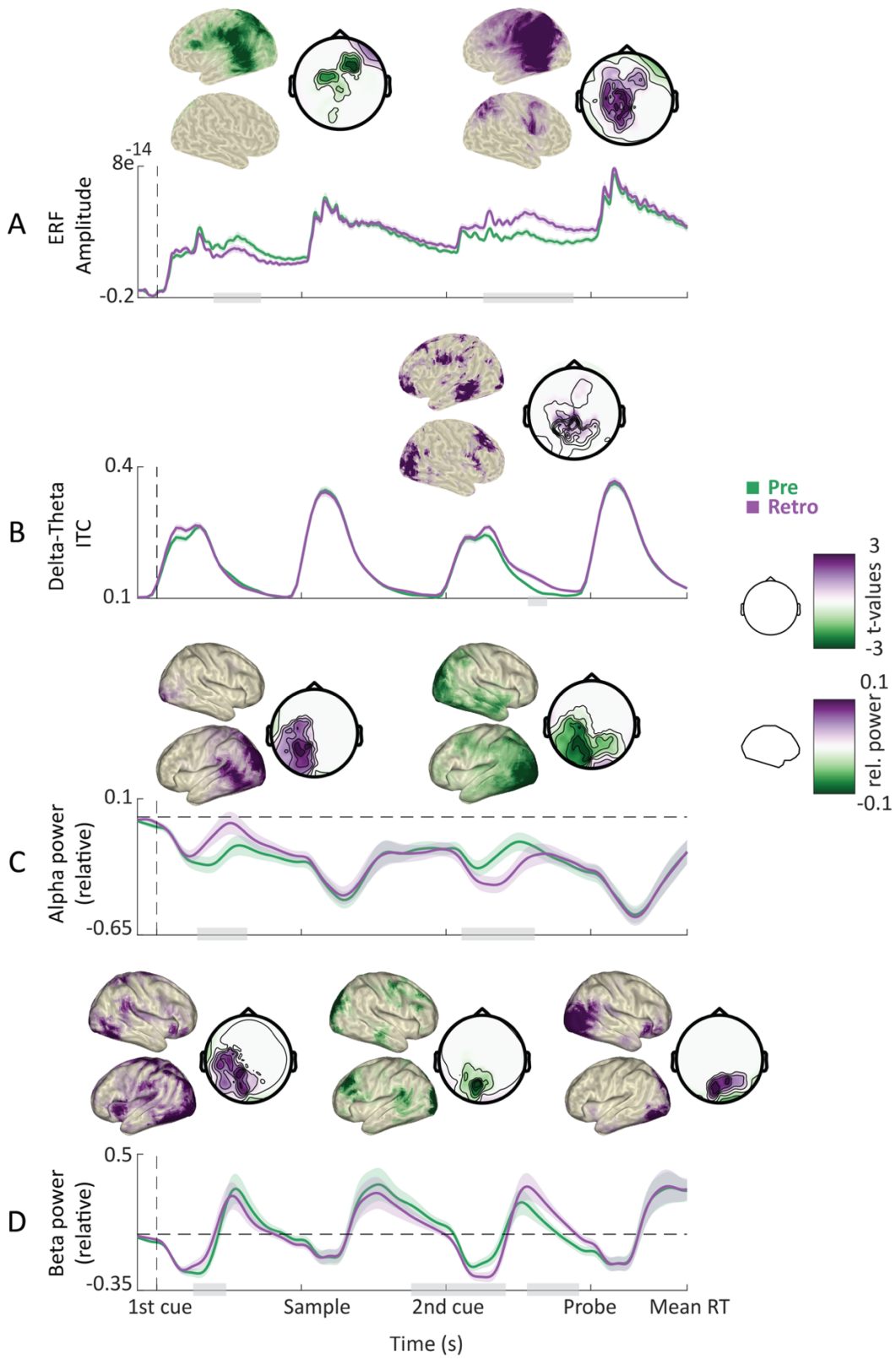
A
ERF
Amplitude
8e-14
-0.2
B
Delta-Theta
ITC
0.4
0.1
Pre
Retro
3
t-values
-3
0.1
rel. power
-0.1
C
Alpha power
(relative)
0.1
-0.65
D
Beta power
(relative)
0.5
-0.35
1st cue
Sample
2nd cue
Probe
Mean RT
Time (s)

**Figure 4**

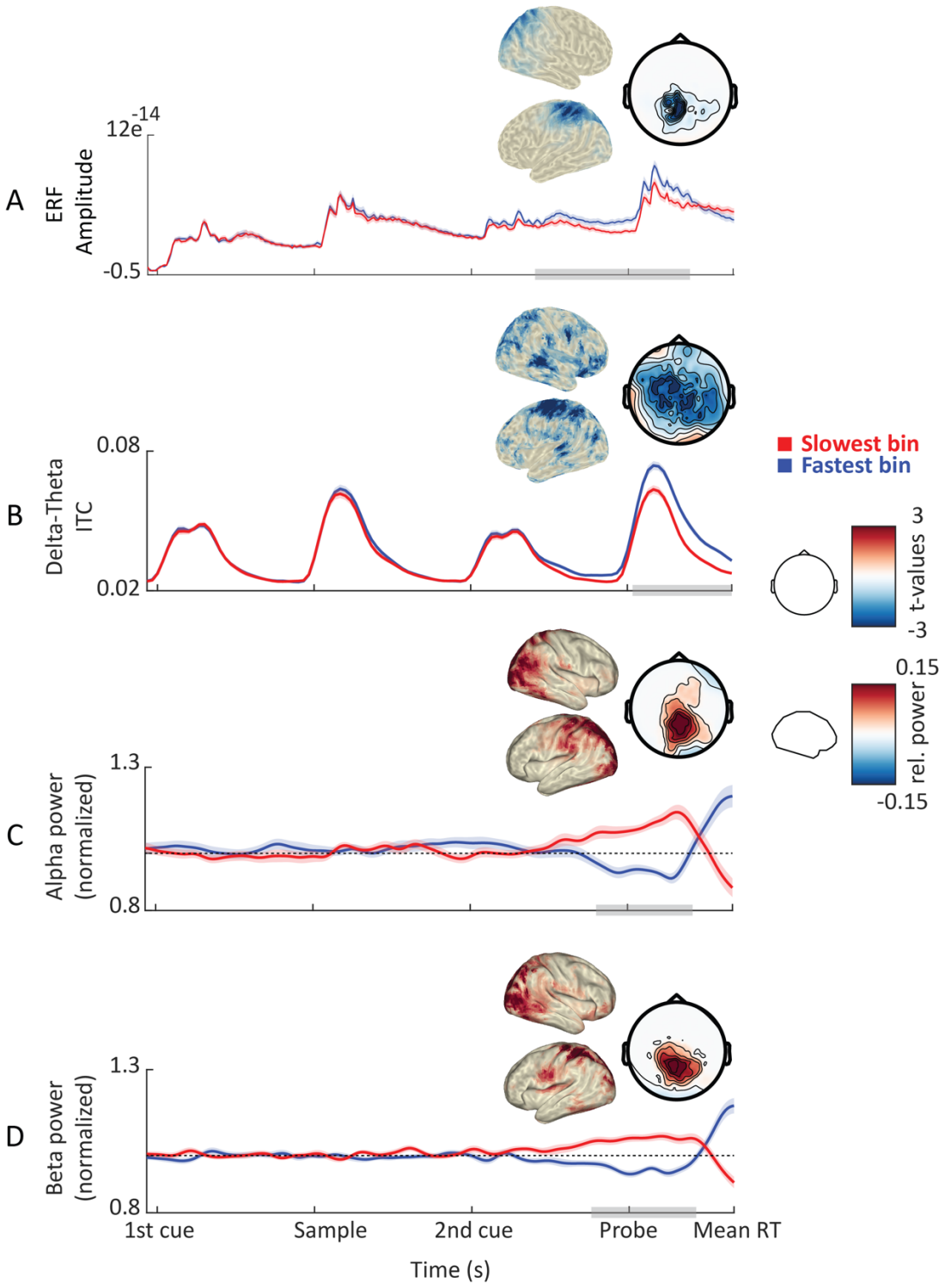
A
ERF
Amplitude
12e-14
-0.5
B
Delta-Theta
ITC
0.08
0.02
Slowest bin
Fastest bin
3
t-values
-3
C
Alpha power
(normalized)
1.3
0.8
0.15
rel. power
-0.15
D
Beta power
(normalized)
1.3
0.8
1st cue
Sample
2nd cue
Probe
Mean RT
Time (s)

**Figure 5**

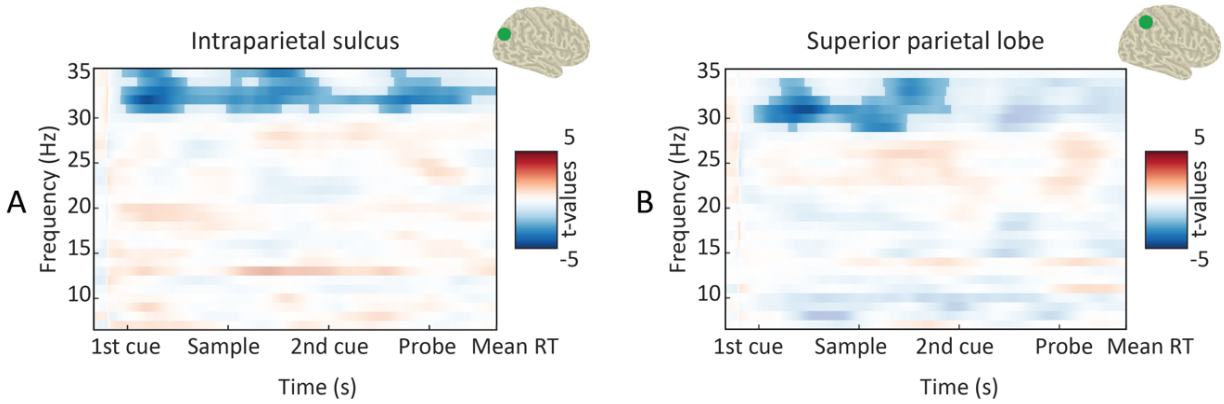


**Figure 6**

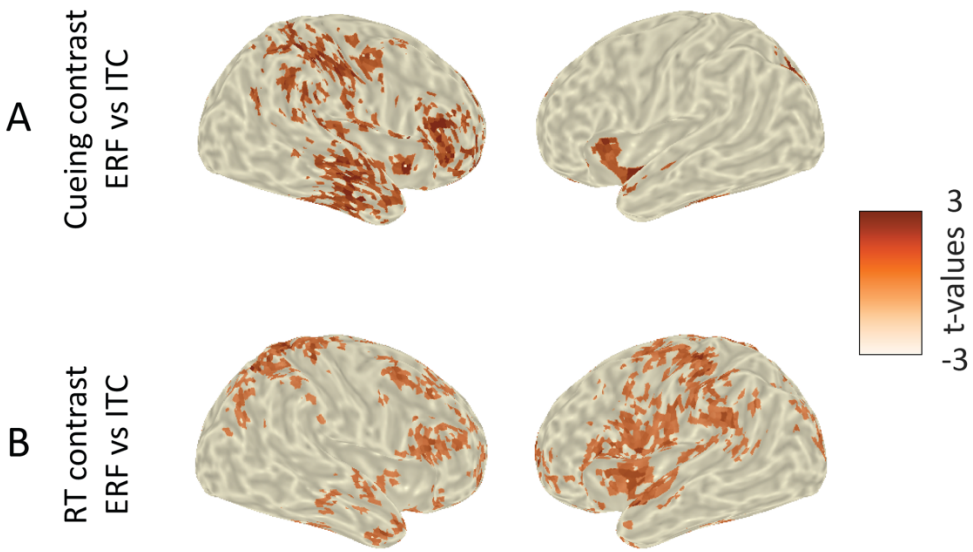


**Figure 7**

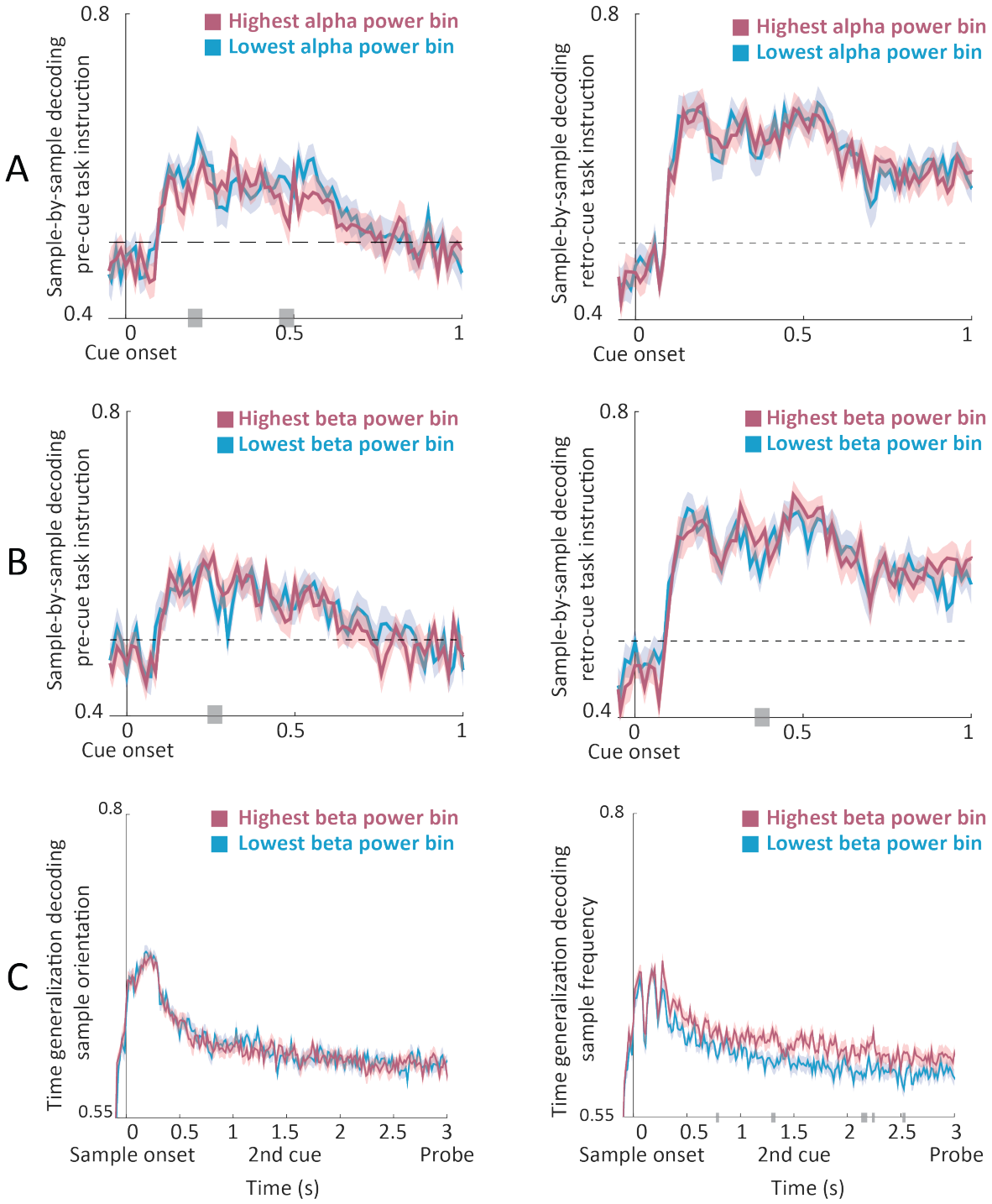


931

932 **Figure 8**